Acceleration Control for Dynamic Manipulation of a Robot Turning Over Objects

Toshiaki Tsuji, Kyo Kutsuzawa, and Sho Sakaino

***Abstract*—This study deals with dynamic object manipulation by a robot using a tool. In order to keep the contact between the held spatula and the manipulated object, a variety of movements satisfying conditions in acceleration dimension should be planned. However, it is quite difficult to assure the acceleration to stay in a certain range in case disturbances exist. Therefore, this study proposes a control architecture for acceleration control and discusses how to develop a controller suitable for dynamic object manipulation. Comparison through simulation and experimental results reveals the features of the proposed control system.**

***Index Terms*—Contact modelling, dexterous manipulation, manipulation planning, motion control, motion control of manipulators.**

I. Introduction

MANY tasks in daily life require humans to dynamically manipulate objects. Dynamic object manipulation has attracted many researchers in robotics because robots may extend their ability by introducing such a technique. Grasping considering dynamics is a popular issue for manipulation [1]–[3]. Many researches have also discussed on kinodynamic constraints, that is, the constraints owing to the physical laws the robots are subject to. Kinodynamic planning methods have been applied to humanoid robots [4], underactuated robots [5], and quadrotor helicopter [6]. A motion planning with acceleration limits have been studied as well [7]. Model predictive control (MPC) is also a well-developed theory, which has an ability to deal with optimal control problems in complicated systems. Therefore, there are examples on motion planning of constrained dynamic systems [8] and biped robots [9], [10]. Hirose *et al.* have developed MPC based kinodynamic control system for an inverted pendulum type personal robot and realized posture stabilization control [11]. Andreasson *et al.* have developed a path smoothing approach based on a lattice-based motion planner for non-holonomic industrial vehicles, highly accurate in real environment [12]. An MPC based omnidirectional robot has shown good performance of tilt recovery [13]. The authors' group has derived the conditions for manipulating an object on a spatula and realized turning over movement of a pancake by a robot holding a spatula [14].

Manuscript received February 15, 2017; accepted June 9, 2017. Date of publication June 28, 2017; date of current version August 15, 2017. This paper was recommended for publication by Associate Editor R. Ozawa and Editor P. Rocco upon evaluation of the reviewers' comments. This work was supported by the Grant-in-Aid for Scientific Research (B), 16H04311. *(Corresponding author: Toshiaki Tsuji.)*

The authors are with the Graduate School of Science and Engineering, Saitama University, Saitama 338-8570, Japan (e-mail: tsuji@ees.saitama-u.ac.jp; s15mm218@mail.saitama-u.ac.jp; sakaino@mail.saitama-u.ac.jp).

Digital Object Identifier 10.1109/LRA.2017.2720848

As many previous studies have shown, kinodynamic planning deals with constraints on acceleration. Although most of the studies have discussed on the way to plan the optimized trajectory, it is also important to discuss the control architecture assuring the command acceleration determined based on the optimized trajectory. PD control or PID control are typical and fundamental solutions for achieving a given trajectory, while acceleration responses may deviate from the constraint condition due to external factors such as disturbance and control delay. Disturbance observer (DOB) is one of the most well-known architecture of acceleration feedback control [15]. Acceleration feedforward control is also well studied in other areas such as precision control [16]. White *et al.* have compared these two methods using the same magnetic disc drive and concluded that DOB offers better results in a low-frequency range, while acceleration feedforward reacts faster [17]. However, there are very few examples combining these two [18] because they deal with similar disturbances. It is guessed that the combination may simply end up with larger vibration due to their conflict. Therefore, this letter discusses a method combining DOB and acceleration feedforward. The solution for avoiding the conflict is to add acceleration command to the DOB as feedforward input, instead of adding measured acceleration. It stands for only feedforwarding inertia force effect of the planned trajectory and such a controller will cover a wider frequency range of the planned trajectory. This study evaluates the acceleration control performance in simulation and clarify the property in view of acceleration tracking performance. Experimental results of movements turning over a pancake also show the performance of the proposed controller and further support the claim.

II. Control Scheme for Dynamic Object Manipulation

This section describes the control scheme for dynamic manipulation. First, MPC for dynamic manipulation is introduced based on the example of turning over pancakes. Second, model of contact between an object and a tool is described for deriving the acceleration limit. Then, the control architecture effective in dynamic manipulation is proposed in the last subsection.

A. Model Predictive Control [20]

This section describes the mechanism of kinodynamic planning for turning over an object. A pancake is selected as a typical object to be turned over. The motion of the object should satisfy the acceleration constraints given by the contact model shown in Fig. 1. Though this study intends for robots in a

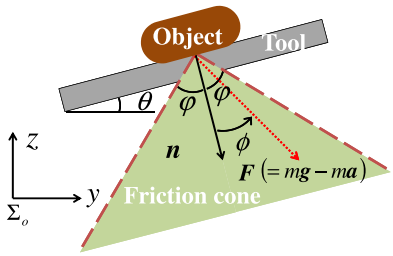

Fig. 1. Force acting on the object placed on a tool.

three-dimensional space, the motion planning scheme is described with movements within a plane, because the turning over movement can be described as movements on a two-dimensional plane. Firstly, the object is modeled as a rigid body and its dynamics is described as follows:

$$\boldsymbol{F} = \boldsymbol{mg} - \boldsymbol{ma} \tag{1}$$

where $\boldsymbol{m} = \mathrm{diag}(m, m, I_\theta)$, $\boldsymbol{a} = [a_y, a_z, a_\theta]^T$, and $\boldsymbol{g} = [0, g_z, 0]^T$. m and I_θ are the mass of the object and MOI in θ rotation, respectively. θ is an inclination angle with respect to the horizontal plane. a is acceleration, while the subscripts y and z denote horizontal and vertical axes. g_z is gravity acceleration.

Although nonlinear MPC schemes are accessible to fast systems requiring short computation times, linear MPC schemes still allow shorter computation times. Under the assumption that the contact between the object and the spatula is maintained, the acceleration of the object will be equal to that of the robot. Additionally, assuming that the controller is accurate enough, response acceleration follows the command acceleration closely. How to assure these two assumptions will be discussed in the latter parts. With the two assumptions, the control model is simplified as follows:

$$\hat{\boldsymbol{x}}(k+1) = \boldsymbol{A}\hat{\boldsymbol{x}}(k) + \boldsymbol{B}\boldsymbol{u}(k) \tag{2}$$

$$\hat{\boldsymbol{x}}(k) = [y(k), z(k), \theta(k), v_y(k), v_z(k), v_\theta(k)]^T \tag{3}$$

$$\hat{\boldsymbol{u}}_{\boldsymbol{k}} = [a_y(k), a_z(k), a_\theta(k)]^T \tag{4}$$

$$\boldsymbol{A} = \begin{bmatrix} 1 & 0 & 0 & \Delta T & 0 & 0 \\ 0 & 1 & 0 & 0 & \Delta T & 0 \\ 0 & 0 & 1 & 0 & 0 & \Delta T \\ 0 & 0 & 0 & 1 & 0 & 0 \\ 0 & 0 & 0 & 0 & 1 & 0 \\ 0 & 0 & 0 & 0 & 0 & 1 \end{bmatrix}$$

$$\boldsymbol{B} = \begin{bmatrix} \Delta T^2/2 & 0 & 0 \\ 0 & \Delta T^2/2 & 0 \\ 0 & 0 & \Delta T^2/2 \\ \Delta T & 0 & 0 \\ 0 & \Delta T & 0 \\ 0 & 0 & \Delta T \end{bmatrix}$$

Here, $\hat{\boldsymbol{x}}_k$ is the kth sample of the state of the object. ΔT is the sampling time.

Since MPC is an effective method to optimize the trajectory under limitation of the input, this study introduces MPC. The proposed MPC method computes a trajectory of the object which minimizes a cost function related with each movement. The cost function J is given as follows:

$$J = (\theta(k_g) - \pi)^2 + \alpha y(k_g)^2 + \beta(v_y(k_g)^2 + v_z(k_g)^2). \tag{5}$$

Here, α and β denote the weighting factors. k_g denotes the sample at which the object (i.e. pancake) touches the ground after the turning over movement.

B. Model of Contact between Object and Tool [14]

Supposing the object on the tool starts to slide on the tool at $\theta \geq \varphi$, the maximum static frictional force $\boldsymbol{F}_{imax}$ is expressed by the following formula, using the static friction coefficient μ:

$$\boldsymbol{F}_{imax} = \mu m \boldsymbol{g} \cos\varphi. \tag{6}$$

The above formula assumes quasi-static rotation. On the other hand, in the turning over movement, the tool will necessarily be in an inclination that exceeds the friction angle φ. In such an instance, some kind of force must be applied to the object to ensure the contact.

The sliding condition of the object is considered by using a friction cone depicted in Fig. 1. If we let the vector perpendicular to the surface of the tool to be $\boldsymbol{n}$ and define the angle created by $\boldsymbol{F}$ and $\boldsymbol{n}$ to be ϕ, then the condition for each contact state can be given in the following manner, by using ϕ:

$$0 \leq \phi < \varphi \tag{7}$$

$$\varphi \leq \phi < \frac{1}{2}\pi \tag{8}$$

$$\frac{1}{2}\pi \leq \phi \tag{9}$$

where (7), (8), and (9) are the conditions for the object in contact without sliding, the object sliding, and the object released from the spatula, respectively.

Conditions of each contact state (7), (8), and (9) are depicted in Fig. 2. The movements on turning over pancakes can be achieved by planning a trajectory that satisfies (7) until the inclination angle θ is over $\frac{1}{2}\pi$. When the condition of (7) are not satisfied, the object slides over the tool with the maximum static frictional force being exceeded. Such a trajectory is planned in some specific cases. For example, in case the pancake should slide on the spatula to lay it on a plate, the trajectory should satisfy (8). The angle ϕ that represents the sliding relationship between the tool and the object shall hereinafter be referred to as the sliding angle ϕ.

The next part describes the way to assure the assumption that the contact between the object and the spatula maintains. Let us consider a situation where the tool is accelerating, as shown in Fig. 3, in order to derive the force vector $\boldsymbol{F}$ that satisfies (7). Let us express the resultant force of the gravitational force acting on the object $m\boldsymbol{g}$ and the inertial force $-m\boldsymbol{a}$ as $m\boldsymbol{i}$.

$$m\boldsymbol{g} + (-m\boldsymbol{a}) = m\boldsymbol{i} \tag{10}$$

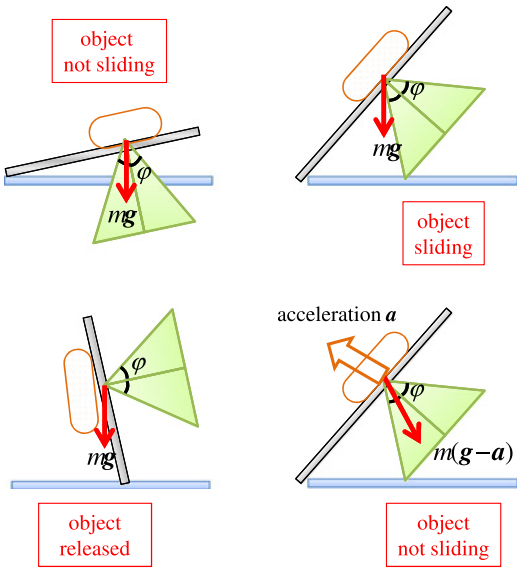

Fig. 2. Relationship between inclination of tool and sliding of object.

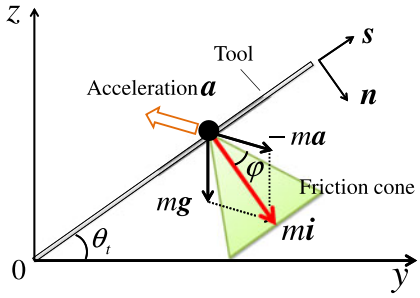

Fig. 3. Reaction force during acceleration and friction cone.

where $\boldsymbol{i}$ is physically expressed in units of acceleration, while $m\boldsymbol{i}$ is equivalent to external force $\boldsymbol{F}$. The vectors parallel and perpendicular to the tool surface are defined as $\boldsymbol{s}$ and $\boldsymbol{n}$, respectively.

The sliding angle ϕ is the angle created by $\boldsymbol{n}$ and $\boldsymbol{i}$. Vector $\boldsymbol{i}$ can be expressed using the following equation:

$$\boldsymbol{i} = \begin{bmatrix} i_y, & i_z \end{bmatrix}^T = \begin{bmatrix} I\sin(\theta_t + \phi), & -I\cos(\theta_t + \phi) \end{bmatrix}^T. \quad (11)$$

where θ_t is θ at time t, and $I = |\boldsymbol{i}|$.

By substituting (11) to (10), the ideal acceleration satisfying desired I and ϕ is derived as follows:

$$\boldsymbol{a} = \begin{bmatrix} a_y, a_z \end{bmatrix}^T = \begin{bmatrix} -I\sin(\theta_t + \phi), g_z + I\cos(\theta_t + \phi) \end{bmatrix}^T. \quad (12)$$

If the acceleration of (12) can be achieved so that ϕ satisfies (7) as described above, turning over motion for any inclination θ_t of the tool becomes possible, without the object sliding on the tool.

C. Control Architecture

The abovementioned trajectory planning method is based on the assumption that the response acceleration is close to the command acceleration since controller is accurate enough. However, it is easily guessed that this assumption may not be valid with an improper control architecture. Therefore, this section proposes control architecture for dynamic object manipulation.

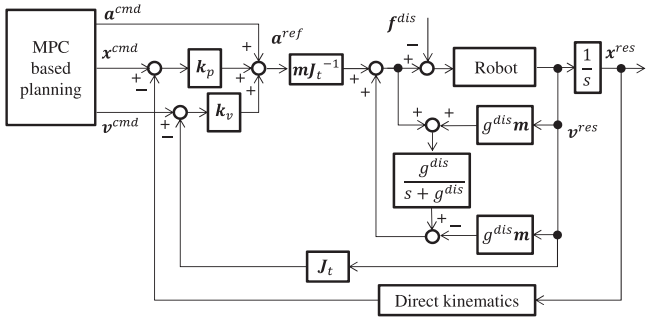

Fig. 4. Block diagram of the proposed controller.

Fig. 4 shows the block diagram of the proposed controller. Here, $\boldsymbol{J}_t$ is a Jacobian matrix of the robot. The MPC plans the trajectory for dynamic object manipulation and generates $\boldsymbol{x}^{cmd}$, $\boldsymbol{v}^{cmd}$, and $\boldsymbol{a}^{cmd}$, position, velocity, and acceleration command, respectively. The feedback controller is a traditional architecture combining PD controller with DOB. The difference is that the acceleration feedforward is added from the MPC planner. Since most of kinodynamic planning methods derive the command trajectory in advance, it is possible to calculate acceleration command. Furthermore, the acceleration feedforward does not contain sensor noise because it is an ideal value calculated by the MPC. The control bandwidth of the acceleration control is simply setup by the cutoff frequency g^{dis}.

In previous methods, the input reference was generated only from position and velocity response, or the acceleration feedforward calculated based on sensor information was added. The acceleration feedforward calculated from the planned trajectory cancels only the inertia force of the robot arm and the all other disturbances are cancelled by the DOB.

III. Verification in Simulation

This section compares the performance of several controllers for acceleration control. First, the conditions for simulation are shown. Next, the property of the controllers are discussed through the simulation results.

A. Conditions of Simulation

Performance of four control architectures were compared through a simplified 1 DOF simulation. The four are: the proposed controller with both FF and DOB; the DOB based controller without FF; the FF controller without DOB; and the controller without both FF and DOB. These controllers are evaluated through 0.1 ms sampling numerical simulations. The parameters were given as follows: $m = 1.0$[kg], $k_p = 900.0$, $k_v = 60.0$, and $g^{dis} = 30.0$[rad/sec].

B. Simulation Results

Fig. 5 compares the frequency responses under the condition without any friction. Gravity force is given as a disturbance ($f^d = mg$). The gain is calculated from the ratio of the response

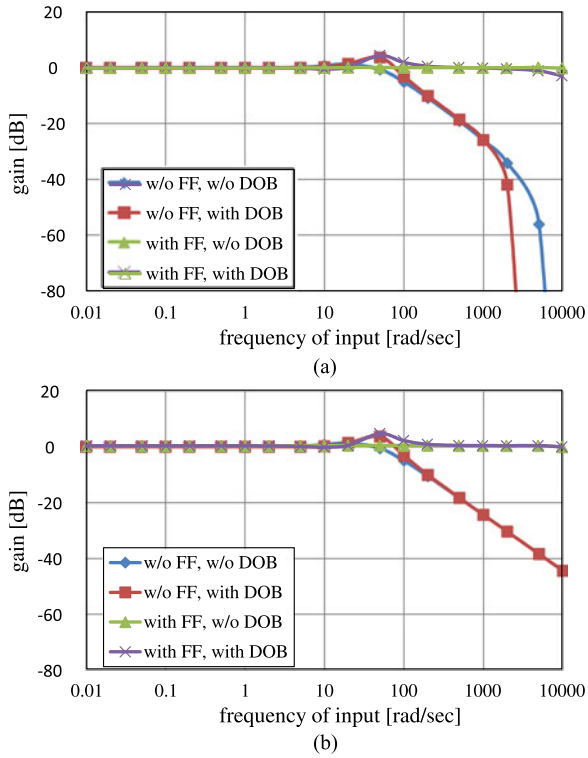

Fig. 5. Frequency response of gain (w/o friction).

amplitude to the command amplitude when

$$x^{cmd} = -\sin \omega t \tag{13}$$

$$v^{cmd} = -\omega \cos \omega t \tag{14}$$

were given to the PD controller as commands.

$$a^{cmd} = \omega^2 \sin \omega t \tag{15}$$

was given as an FF input, then.

The results show that acceleration responses follow the acceleration command in the lower frequency range when a simple PD controller is implemented. By adding a DOB, the control bandwidth is extended a bit. On the other hand, FF inputs widely extend the control bandwidth in theory.

Fig. 6 compares the frequency responses under the condition with friction. The disturbance force is given as $f^d = mg + f(v)$, where $f(v) = -sgn(v)f_c - dv$, $d = 0.1$[Ns/m]. Here, $f_c = 0.1$[N] is the static friction on the joint. The properties of the controller confirmed from the results were similar to that of Fig. 5, while the acceleration amplitudes were larger in lower frequency range. The acceleration amplitudes became larger due to the stick-slip phenomenon caused by the static friction f_c. As it is clear from (15), the amplitude of acceleration input is very small in lower frequency range. On the other hand, the acceleration of stick-slip phenomenon is about the same in any frequency ranges. As a result, the gain is larger in lower frequency range. This result infers that the performance of kinodynamic planning may deteriorate with a large static friction.

Fig. 7 compares the root mean squared error (RMSE) of position control. The DOB reduces the position error in the low

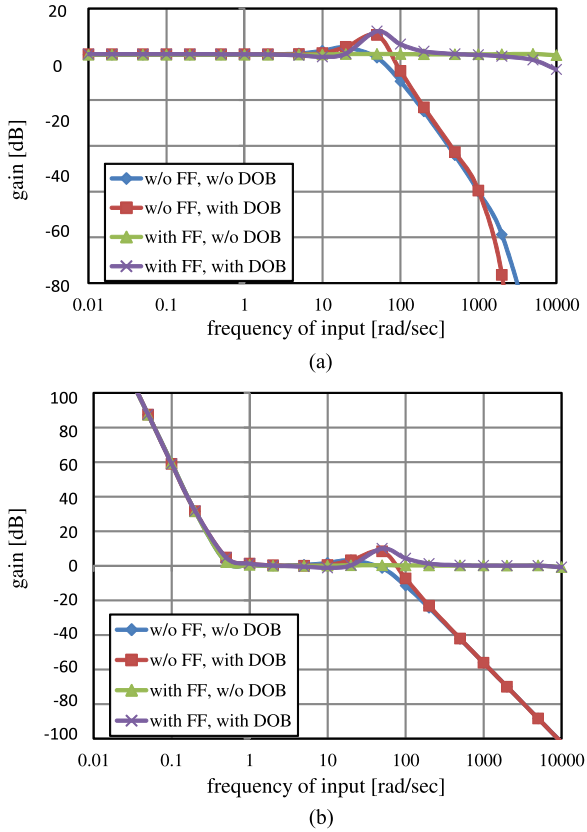

Fig. 6. Frequency response of gain (with friction).

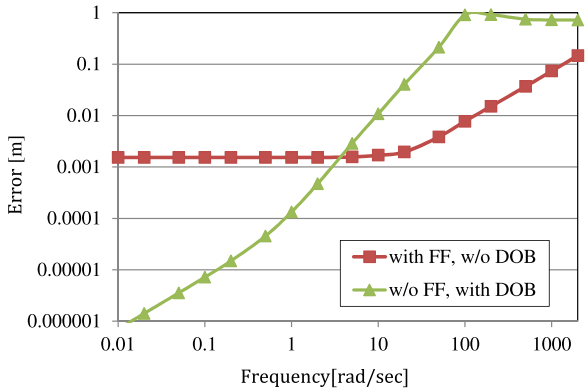

Fig. 7. Frequency response of root mean squared error.

frequency range, while the error is larger in the high frequency range. FF control has larger error in the low frequency range, which is mainly caused by the gravity term. On the other hand, the FF control still keeps the performance in the high frequency range.

Fig. 8 compares the delay in each control architecture. The results over 5000 rad/sec frequency are not shown because they had low reproducibility depending on the condition. The results in Fig. 8(a) support that the control bandwidth with small phase lag is extended by adding DOB. As the cutoff frequency of the DOB is enlarged, the control bandwidth is extended. The phase lag results also indicate that FF input widely extends the control bandwidth. One interesting result is that the combination of FF

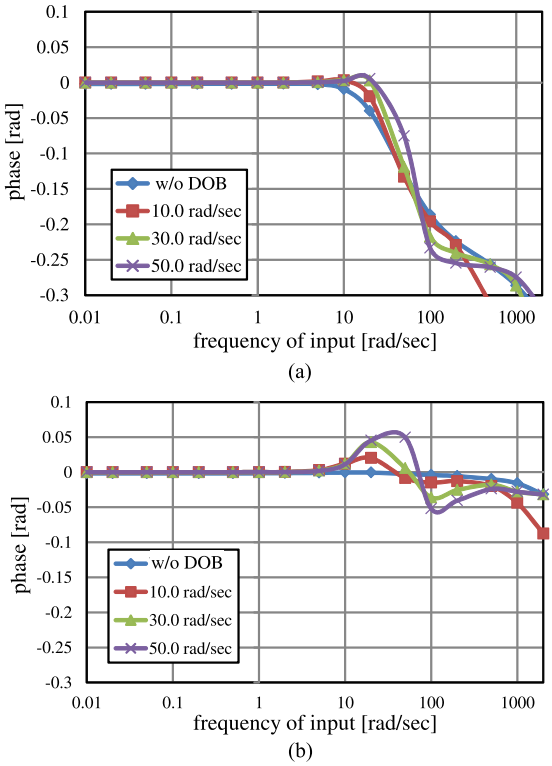

Fig. 8. Frequency response of phase (with friction).

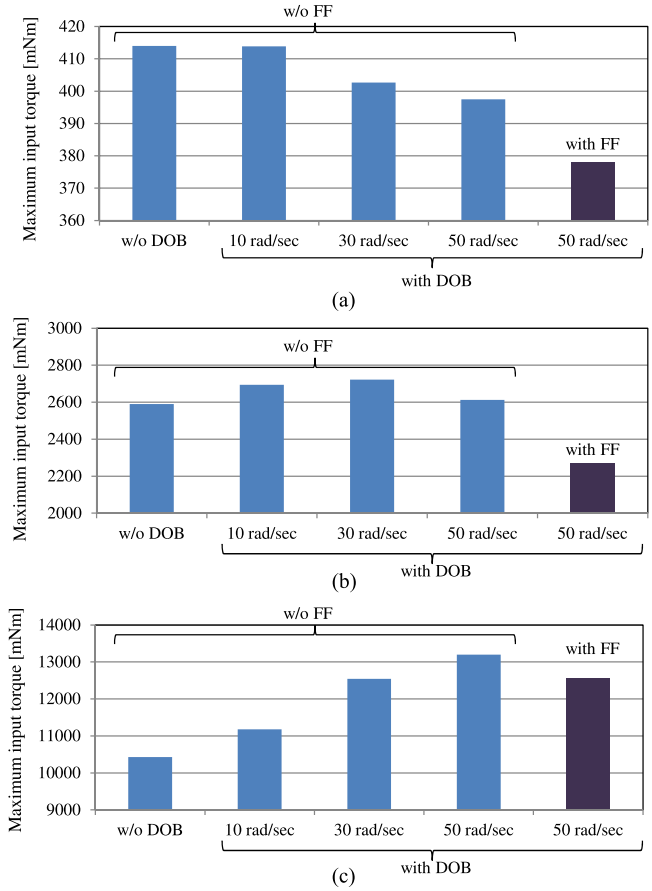

Fig. 9. Maximum input torque of different controllers.

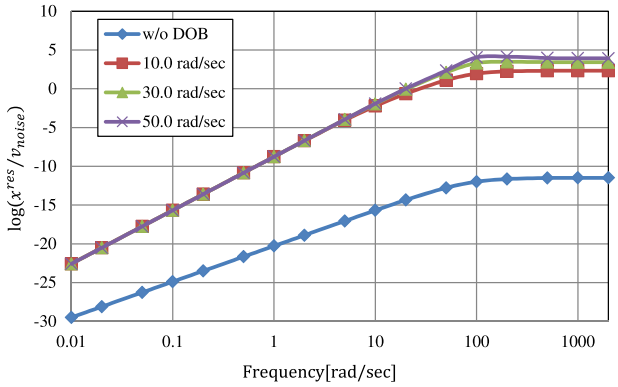

Fig. 10. Frequency response of noise gains.

and DOB shows phase lead in the middle frequency range. It is well known that FF reduces the phase lag, and it is also known that DOB has similar effect [15]. Combination of the two delay compensation leads the phase lead.

Fig. 9 compares the amplitude of input torque of several control architectures. The maximum value of input torque during steady state was measured, while the position command was given by a sinusoidal function. Since the higher frequency position command results in higher acceleration, the maximum input torque is smaller in Fig. 9(a) and larger in Fig. 9(c). Fig. 9(a) shows that the maximum torque decreases as the cutoff frequency of DOB g^{dis} increases. If the frequency of the command is lower than g^{dis}, the maximum torque decreases as the control performance improves with higher g^{dis}. On the other hand, Fig. 9(c) shows the opposite results. The maximum input torque increases as the cutoff frequency of DOB g^{dis} increases because the DOB generates vibration in case frequency of the command exceeds g^{dis} and the vibration is larger with higher g^{dis}. In all these results, the maximum input torque was smaller with FF input. As shown in Fig. 6, the FF input does not decrease the vibration generated by DOB, while the phase lead FF input reduces maximum torque by recovering the phase delay.

Fig. 10 shows the frequency response of noise gains. In the simulation, the position command was set as $x^{cmd} = 0$. Velocity measurement noise v^{noise} generated by sinusoidal function was added to v^{res} in the controller in Fig. 4. Then, the PD controller and DOB produced some vibration due to the measurement noise. The amplitude to noise ratio x^{res}/v^{noise} was measured and compared. The figure shows that DOB excites vibration due to the measurement noise and higher cutoff frequency of DOB g^{dis} results in larger vibration. FF input does not have this affect at all since it is not related with measurement noise.

Summarizing the results in Figs. 9 and 10, the combination of DOB and FF results in high control bandwidth with smaller torque input. DOB itself much improves the control performance, while it has a negative effect on exciting vibration. FF input extends the control bandwidth and it also reduces the input torque by the phase lead effect.

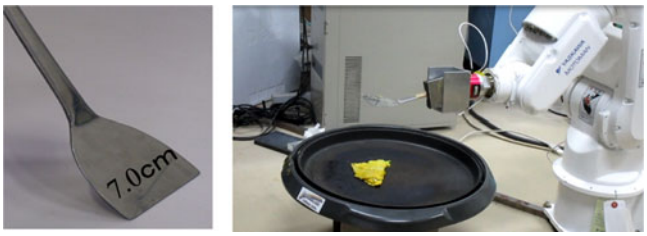

Fig. 11. Experimental setup.

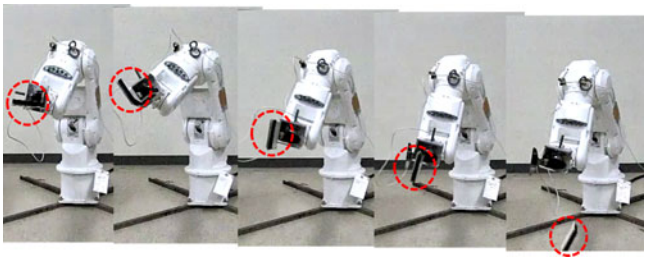

Fig. 12. Snapshots of turning over motion.

IV. Verification Through Experiment

A. System Configuration of the Robot

This study used a 6-DOF manipulator "Motoman-MH3F," from Yaskawa Electric. Fig. 11 shows the photo with a spatula fixed at the tip of the manipulator. PD controller with disturbance observer was implemented. Its sampling time was 1 ms and the parameters of the MPC and the feedback controller were as follows: $\alpha = 20.0$, $\beta = 0.5$, $\boldsymbol{k}_p = \mathrm{diag}[350, 350, 350]^T$, $\boldsymbol{k}_v = \mathrm{diag}[120, 120, 120]^T$, and $g^{dis} = 12.6$.

In order to have an evaluation with high reproducibility, a rubber block ($65 \times 62 \times 10$ mm) was used as the object instead of real pancakes. The weight of the block was 61 g. The static friction of the block was adjusted so that it is about the same to that of real pancakes. The static friction coefficient was measured 10 times and the average value was 1.86.

B. Experimental Results

Fig. 12 shows the snapshots of turning over motion of the robot with the proposed method implementing both FF and DOB. By MPC under the constraint of acceleration input, turning over trajectory is automatically generated. Fig. 13 compares the trajectories of the spatula with different control architectures. Since the gravity term was compensated with the DOB, DOB based controllers had much smaller error from the command trajectory. Two controllers: with both FF and DOB, and with DOB without FF, were successful with turning over motion. It was judged as success when the object angle at the touch down was larger than $\frac{1}{2}\pi$ and smaller than $\frac{3}{2}\pi$. On the other hand, two controllers without DOB failed with the turning over motion. The object slid and fell down at the beginning of turning over motion with both controllers. As it is known from the previous studies, feedback control is effective in the experimental system with large and unpredictable disturbances. Fig. 14 compares the velocity of the spatula of two successful results. The controller

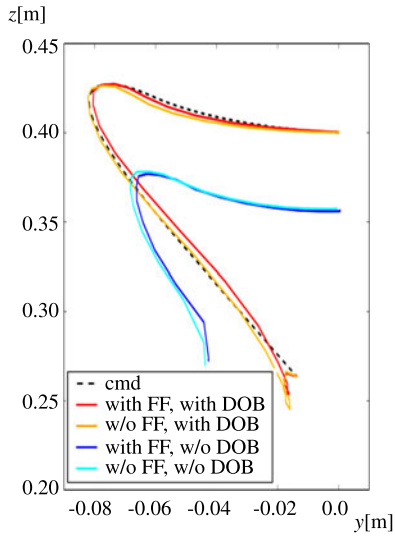

Fig. 13. Turning over trajectories.

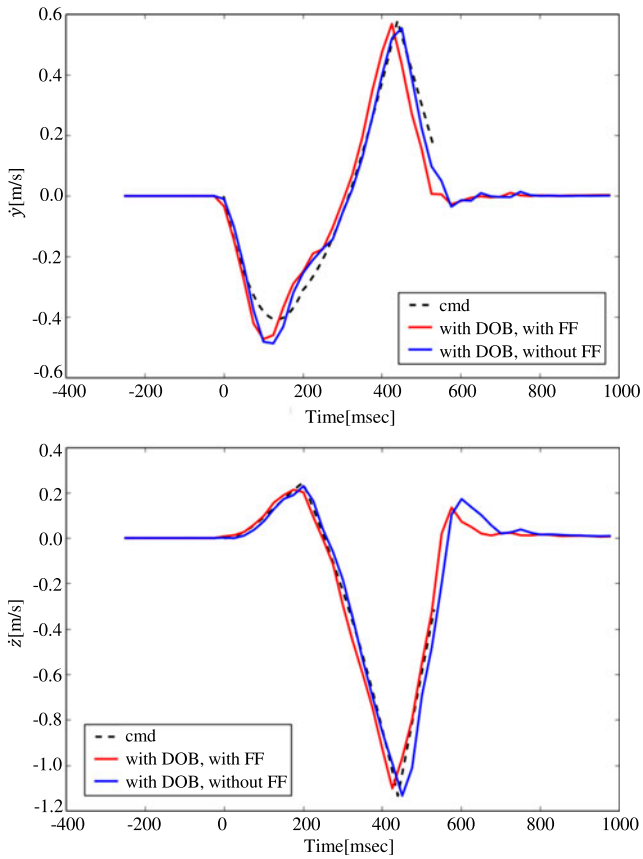

Fig. 14. Velocity response.

with DOB without FF had slight lag, while the controller with both DOB and FF had slight phase lead. This result supports that the combination of two methods leads to phase lead in a specific frequency range.

Although the result with acceleration FF input did not show a significant difference at a glance, one small noticeable difference is observed in the experimental result. The result without FF shows vibration around the endpoint of the trajectory while

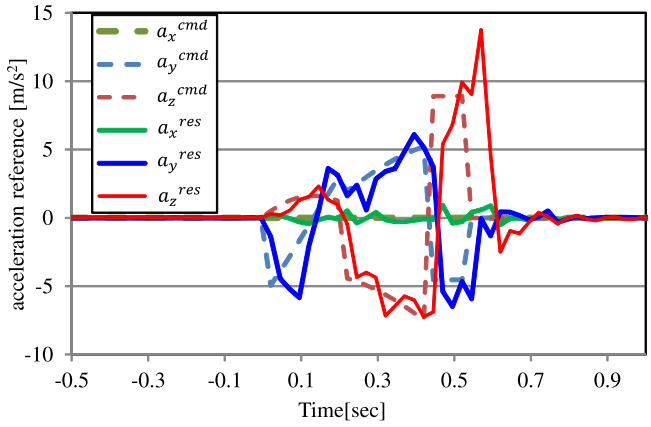

Fig. 15. Acceleration references.

the vibration was less in the result with FF. The difference is also seen in the trajectory response in Fig. 13. When the trajectory planning by the MPC ended, the velocity response was reduced to zero immediately. Due to the immediate reduction, high frequency components larger than the cutoff frequency of DOB occurred in the command response. Therefore, the high frequency components generated vibration. Since the FF input does not have limitation of control bandwidth, the vibration was much smaller. As the velocity responses in Fig. 14 show, the trajectory of turning over motion calculated by the MPC did not include much high frequency component of acceleration. Therefore, the feedback control worked properly and the turning over motion was accomplished except at the end of the motion.

Without DOB, it should be still possible to further extend the control bandwidth by heightening feedback PD gains, while such attempt failed in this control system due to vibrations. Hence, the results indicate that PD controller with DOB shows better performance than a simple PD controller in kinodynamic planning.

Fig. 15 shows the acceleration responses during the turning over motion. The acceleration commands produced by the MPC based planner are also shown. The results show that acceleration responses follow the commands well. Note that tracking performance of acceleration is lower than that of position in general. The appropriate combination of feedforward and feedback inputs can suppress disturbance and furthermore, it also follows command with higher requency components.

The turning over motion was tested with 8 different initial positions to verify the performance with different positions. The initial position of the first trial was at the center of the workspace. Then, the initial position was moved 2 cm away on the y-axis in the next trial. The initial position of the last trial was 14 cm away on the y-axis from the center of workspace. The average RMSE was 1.10 cm with 0.15 cm standard deviation. The RMSE of the last trial was 1.18 cm and therefore, it can be concluded that the performance does not change much as long as the planned trajectory is within the workspace. The average RMSE of acceleration was 4.65 m/sec^2 while the RMSE of the result without FF was 4.81 m/sec^2. The maximum torque of the motor on the second joint, which bears the largest load, was 205 Nm (load side), while the result without FF was 224 Nm. These results coincide with the results in simulation and support the claim that the combination of FF and DOB shows good performance for dynamic manipulation.

V. Conclusion

Turning over a pancake is a good candidate for evaluating performance of dynamic object manipulation, since it is a typical example of motion with kinodynamic constraints and it also requires a rapid response. Since acceleration is the key factor for kinodynamic constraints, this study discussed the property of an acceleration control architecture for MPC based kinodynamic planning. The results of simulations and experiments reveal the following properties of acceleration control architectures.

1) Both DOB and acceleration FF have an effect to reduce the delay and they extend the control bandwidth of acceleration control.
2) FF is effective in an environment with small disturbances, while a feedback control by DOB is more effective in real environment with larger unpredictable disturbances.
3) Combination of DOB and FF is effective in case the command trajectory includes high frequency components. It was also confirmed that the proposed method results in phase lead in a certain frequency range because both control have the delay compensation property.

References

[1] K. Tahara, S. Arimoto, and M. Yoshida, "Dynamic object manipulation using a virtual frame by a triple soft-fingered robotic hand," in *Proc. IEEE Int. Conf. Robot. Autom.*, 2010, pp. 4322–4327.
[2] Y. Bekiroglu, J. Laaksonen, J. A. Jorgensen, V. Kyrki, and D. Kragic, "Assessing grasp stability based on learning and haptic data," *IEEE Trans. Robot.*, vol. 27, no. 3, pp. 616–629, Jun. 2011.
[3] M. Li, Y. Bekiroglu, D. Kragic, and A. Billard, "Learning of grasp adaptation through experience and tactile sensing," in *Proc. IEEE/RSJ Int. Conf. Intell. Robots Syst.*, 2014, pp. 3339–3346.
[4] J. J. Kuffner, S. Kagami, K. Nishiwaki, M. Inaba, and H. Inoue, "Dynamically-stable motion planning for humanoid robots," *Auton. Robots*, vol. 12, no. 1, pp. 105–118, 2002.
[5] G. Goretkin, A. Perez, R. Platt, and G. Konidaris, "Optimal sampling-based planning for linear-quadratic kinodynamic systems," in *Proc. IEEE Int. Conf. Robot. Autom.*, 2013, pp. 2429–2436.
[6] D. Webb and J. van den Berg, "Kinodynamic RRT*: Asymptotically optimal motion planning for robots with linear dynamics," in *Proc. IEEE Int. Conf. Robot. Autom.*, 2013, pp. 5054–5061.
[7] T. Kunz and M. Stilman, "Probabilistically complete kinodynamic planning for robot manipulators with acceleration limits," in *Proc. IEEE/RSJ Int. Conf. Intell. Robots Syst.*, 2014, pp. 3713–3719.
[8] D. Nguyen-Tuong and J. Peters, "Model learning for robot control: A survey," *Cogn. Process.*, vol. 12, no. 4, pp. 319–340, 2011.
[9] P. B. Wieber, "Trajectory free linear model predictive control for stable walking in the presence of strong perturbations," in *Proc. 6th IEEE-RAS Int. Conf. Humanoid Robots*, 2006, pp. 137–142.
[10] H. Diedam, D. Dimitrov, P. B. Wieber, K. Mombaur, and M. Diehl, "Online walking gait generation with adaptive foot positioning through linear model predictive control," in *Proc. IEEE/RSJ Int. Conf. Intell. Robots Syst.*, 2008, pp. 1121–1126.
[11] N. Hirose, R. Tajima, and K. Sukigara, "Personal robot assisting transportation to support active human life—Following control based on model predictive control with multiple future predictions," in *Proc. IEEE/RSJ Int. Conf. Intell. Robots Syst.*, 2015, pp. 5395–5402.

[12] H. Andreasson, J. Saarinen, M. Cirillo, T. Stoyanov, and A. J. Lilienthal, "Fast, continuous state path smoothing to improve navigation accuracy," in *Proc. IEEE Int. Conf. Robot. Autom.*, 2015, pp. 662–669.

[13] J. Lafaye, C. Collette, and P. B. Wieber, "Model predictive control for tilt recovery of an omnidirectional wheeled humanoid robot," in *Proc. IEEE Int. Conf. Robot. Autom.*, 2015, pp. 5134–5139.

[14] T. Tsuji, J. Okuma, and S. Sakaino, "Dynamic object manipulation considering contact condition of robot with tool," *IEEE Trans. Ind. Electron.*, vol. 63, no. 3, pp. 1972–1980, Mar. 2016.

[15] T. Murakami, F. Yu, and K. Ohnishi, "Torque sensorless control in multidegree-of-freedom manipulator," *IEEE Trans. Ind. Electron.*, vol. 40, no. 2, pp. 259–265, Apr. 1993.

[16] M. T. White and M. Tomizuka, "Increased disturbance rejection in magnetic disk drives by acceleration feedforward control and parameter adaptation," *Control Eng. Pract.*, vol. 5, no. 6, pp. 741–751, 1997.

[17] M. T. White, M. Tomizuka, and C. Smith, "Improved track following in magnetic disk drives using a disturbance observer," *IEEE/ASME Trans. Mechatronics*, vol. 5, no. 1, pp. 3–11, Mar. 2000.

[18] K. Ohnishi, M. Shibata, and T. Murakami, "Motion control for advanced mechatronics," *IEEE/ASME Trans. Mechatronics*, vol. 1, no. 1, pp. 56–67, Mar. 1996.

[19] Z. Jamaludin, H. Van Brussel, G. Pipeleers, and J. Swevers, "Accurate motion control of xy high-speed linear drives using friction model feedforward and cutting forces estimation," *CIRP Ann., Manuf. Technol.*, vol. 57, no. 1, pp. 403–406, 2008.

[20] T. Tsuji, K. Kutsuzawa, and S. Sakaino, "Optimized trajectory generation based on model predictive control for turning over pancakes," in *Proc. Papers IEEJ Tech. Meet. Mechatronics Control*, 2016, Paper MEC-16-014.

[21] S. Karaman and E. Frazzoli, "Sampling-based algorithms for optimal motion planning," *Int. J. Robot. Res.*, vol. 30, no. 7, pp. 846–894, 2011.